Research Square

Preprints are preliminary reports that have not undergone peer review.
They should not be considered conclusive, used to inform clinical practice,
or referenced by the media as validated information.

GIS-Integrated Plant–Sediment Assessment of Trace-Element Partitioning and FTIR Functional-Group Signatures in Al-Chibayish Marshes, Southern Iraq

Afrah L. Mohammed[1]
[1]Scientific Research Commission
Raghad Mouhamad
raghad.s.mouhamad@src.edu.iq

[1]Scientific Research Commission

Research Article

Keywords: Al-Chibayish Marshes, Mesopotamian Marshes, trace elements, FTIR, plant-sediment interface, wetland geochemistry, organic matter, remote sensing, drying-rewetting

Posted Date: August 12th, 2026

DOI: https://doi.org/10.21203/rs.3.rs-10338674/v1

License: This work is licensed under a Creative Commons Attribution 4.0 International License.
Read Full License

Additional Declarations: No competing interests reported.

GIS-Integrated Plant–Sediment Assessment of Trace-Element Partitioning and FTIR Functional-Group Signatures in Al-Chibayish Marshes, Southern Iraq

Afrah L. Mohammed[1], Raghad Mouhamad[1]

[1]Scientific Research Commission, Baghdad, Iraq

Corresponding author: raghad1974@yahoo.com; raghad.s.mouhamad@src.edu.iq

Abstract

The Al-Chibayish Marshes of southern Iraq form a shallow wetland environment where aquatic plants, roots, buried organic residues and bottom sediment interact as coupled biotic-abiotic compartments controlling trace-element retention. This study presents an original plant-sediment geochemical assessment based on author-generated elemental data, original Tensor 27 FTIR spectra and remote-sensing environmental context. The analytical design uses the laboratory sample names Aziza, Typha root, Typha stem, Typha leaves, Jolan, Tarfa, Shamblan and Bottom sediment. Trace elements showed strong matrix-specific partitioning. Shamblan (Ceratophyllum sp.) had the highest Cd, Ni, Li, Cu and Mn concentrations, reaching 70.6, 73.6, 61.8, 48.1 and 409 mg kg-1, respectively. Bottom sediment contained the highest As, Se, Co, Ca and ash, reaching 179 mg kg-1 As, 88.6 mg kg-1 Se, 21.9 mg kg-1 Co, 63,350 mg kg-1 Ca and 55.48% ash. Typha root showed the strongest root-zone signal for Cr, Fe and Pb. FTIR spectra indicated hydroxyl, aliphatic, carbonyl/amide, ether/methoxy, sulfur-associated and fingerprint-region features that are relevant to organic-matter transformation and contaminant-binding capacity. Satellite-derived NDVI, NDWI/MNDWI, NDMI, LST, BSI, inundation frequency and sediment exposure frequency were used only to describe hydrological and ecological context. The results support a conservative model in which submerged macrophytes, emergent roots and mineral-rich sediment form linked retention compartments whose behavior can shift during inundation, exposure and drying-rewetting cycles.

Keywords: Al-Chibayish Marshes; Mesopotamian Marshes; trace elements; FTIR; plant-sediment interface; wetland geochemistry; organic matter; remote sensing; drying-rewetting.

1. Introduction

Wetlands are reactive geochemical systems in which water, plant tissues, roots, detritus, fine sediment and mineral phases jointly regulate the fate of trace elements and organic matter. In shallow marshes, contaminant storage cannot be understood from the water column alone because particle-reactive elements may be transferred into submerged macrophytes, root coatings, biofilms, organic residues and sediment-associated mineral phases [1-6].

The Mesopotamian Marshes of southern Iraq have undergone major hydrological modification, drainage, reflooding and continuing water-scarcity stress. In the Al-Chibayish sector, repeated inundation and exposure create a dynamic interface where plant-derived organic matter can be transformed during burial and where redox-sensitive elements may be retained or redistributed [7-12]. The system therefore provides a useful field setting for evaluating contaminant behavior across biotic and abiotic matrices.

Organic matter is central to this behavior. Hydroxyl, carbonyl, amide, ether, methoxy, aliphatic and sulfur-associated functional groups can provide sites for sorption, surface complexation, cation bridging and organo-mineral association [13-18]. Mid-infrared FTIR spectroscopy is suitable for screening these functional groups and for comparing organic-matter transformation among plants, residues and sediment. In this manuscript, FTIR evidence is used only at the functional-group level; individual molecular assignments are not made from FTIR alone.

Remote sensing contributes a second, landscape-scale layer by describing vegetation persistence, water extent, surface moisture, thermal stress and sediment exposure [19-25]. Such indicators are not chemical measurements, but they are

relevant because hydrological persistence and drying-rewetting cycles regulate oxygen availability, salinity concentration, organic-matter decomposition and the potential redistribution of sediment-bound elements.

The objectives were to: (i) quantify trace-element partitioning among Aziza, Typha root, Typha stem, Typha leaves, Jolan, Tarfa, Shamblan and Bottom sediment; (ii) identify matrix-specific retention signals for Cd, Ni, Cr, Pb, As, Se, Fe, Mn, Ca and Mg; (iii) interpret FTIR functional groups relevant to organic-matter transformation and contaminant retention; and (iv) integrate remote-sensing context without using satellite indices as direct predictors of chemical concentrations.

2. Materials and methods

2.1 Study area and evidence design

The study focused on Al-Chibayish Marshes, southern Iraq. The manuscript is built from three data streams supplied by the authors: a plant and sediment elemental dataset, original FTIR spectral outputs, and remote-sensing maps/indices describing hydrological variation. The chemical interpretation is based on the laboratory dataset; the remote-sensing component is used as environmental context for hydrological exposure and wetting-drying behavior.

2.2 Sample names and matrices

The manuscript uses the laboratory sample names recorded in the supplied dataset. The term 'Bottom sediment' is used for the sediment matrix, whereas plant matrices are reported by their laboratory names and scientific names where provided. No alternative taxonomic name is introduced for the sediment matrix.

Table 1. Laboratory sample names and matrix descriptions used throughout the manuscript.

Code	Laboratory sample name	Scientific name or matrix	Description
S1	Aziza	Salvinia natans	floating aquatic plant
S2	Typha root	Typha australis root	emergent root tissue
S3	Typha stem	Typha australis stem	emergent stem / buried residue label
S4	Typha leaves	Typha australis leaves	emergent leaf tissue
S5	Jolan	Schoenoplectus litoralis	emergent sedge
S6	Tarfa	Tamarix arabica	riparian halophyte/shrub tissue
S7	Shamblan	Ceratophyllum sp.	submerged macrophyte
S8	Bottom sediment	bottom sediment	bottom sediment matrix

2.3 Elemental composition and calculations

Elemental concentrations were taken from the supplied laboratory worksheet and are reported as mg kg-1, except for N and proximate composition variables that are expressed as percentages. The dataset includes Zn, Cu, Ni, Co, Fe, Mn, Cr, Ca, Mg, K, Na, Li, Pb, Cd, Mo, Se, As and P. LSD0.05 thresholds provided in the worksheet were used only as supplied comparison thresholds; no additional inferential statistics were invented.

$$\textit{Plant-sediment quotient (PSQ)} = C_{plant} / C_{bottom\ sediment}$$

The PSQ is descriptive and is used to compare plant-associated concentrations with the bottom sediment concentration of the same element. It is not treated as a regulatory bioaccumulation factor because matched uptake experiments were not part of the supplied dataset.

2.4 FTIR functional-group interpretation

Mid-infrared FTIR spectra were produced with a Tensor 27 system, as documented in the original FTIR files. Spectral interpretation was restricted to broad functional regions: O-H/hydroxyl, aliphatic C-H, carbonyl/amide, ether/methoxy, sulfur-associated features and the fingerprint region. Library descriptors were treated as screening terms rather than

definitive molecular identifications. The analysis therefore links FTIR patterns to binding environments and organic-matter transformation, not to confirmed individual organic compounds.

2.5 Remote-sensing context

The supplied remote-sensing component used Google Earth Engine and wetland indicators including NDVI, NDWI/MNDWI, NDMI, LST, BSI, inundation frequency and sediment exposure frequency. These indices were used to summarize vegetation-water-exposure conditions and the sequence of wetting, reflooding, exposure and partial recovery from 2000 to 2026. They were not used to estimate metal concentrations.

3. Results

3.1 Trace-element partitioning

Trace-element concentrations were strongly compartmentalized. Shamblan had the highest Cd, Ni, Li, Cu and Mn. Bottom sediment had the highest As, Se, Co, Ca and ash. Typha root had the highest Cr, Fe and Pb among the plant matrices. These patterns show that submerged vegetation, emergent roots and sediment represent distinct geochemical compartments rather than interchangeable sample types.

Table 2. Trace-element concentrations in plant and bottom sediment matrices (mg kg-1).

Sample	Cd	Ni	Cr	Pb	As	Se	Co	Cu	Zn	Mn	Li	Fe
Aziza	4.15	31.5	20.6	30.5	53	39.9	11.9	31.9	47.3	138	4.42	1130
Typha root	8.13	48.7	43.9	63.8	11	85	8.21	41.7	44.6	211	14.9	7780
Typha stem	3.28	9.6	17.9	23.3	39.9	29.2	5.08	22.2	19.7	64.1	2.89	862
Typha leaves	5.48	20.6	25.2	36.9	65.5	48.5	11.5	33.9	27.9	240	5.67	2770
Jolan	3.59	11.4	20.8	25.2	45.5	33.7	6.03	28.2	21.3	150	5.11	1160
Tarfa	4.97	16	22.4	28.1	48.2	37.5	7.66	34.5	47.2	47.9	5.29	992
Shamblan	70.6	73.6	352	50.1	105	73.1	15.4	48.1	31	409	61.8	2810
Bottom sediment	6.11	20.7	25.9	61.6	179	88.6	21.9	22	11.4	74.9	2.97	699
LSD0.05	0.51	23.82	14.06	14.55	9.03	17.41	2.08	10.23	3.06	34.11	1.08	76.31

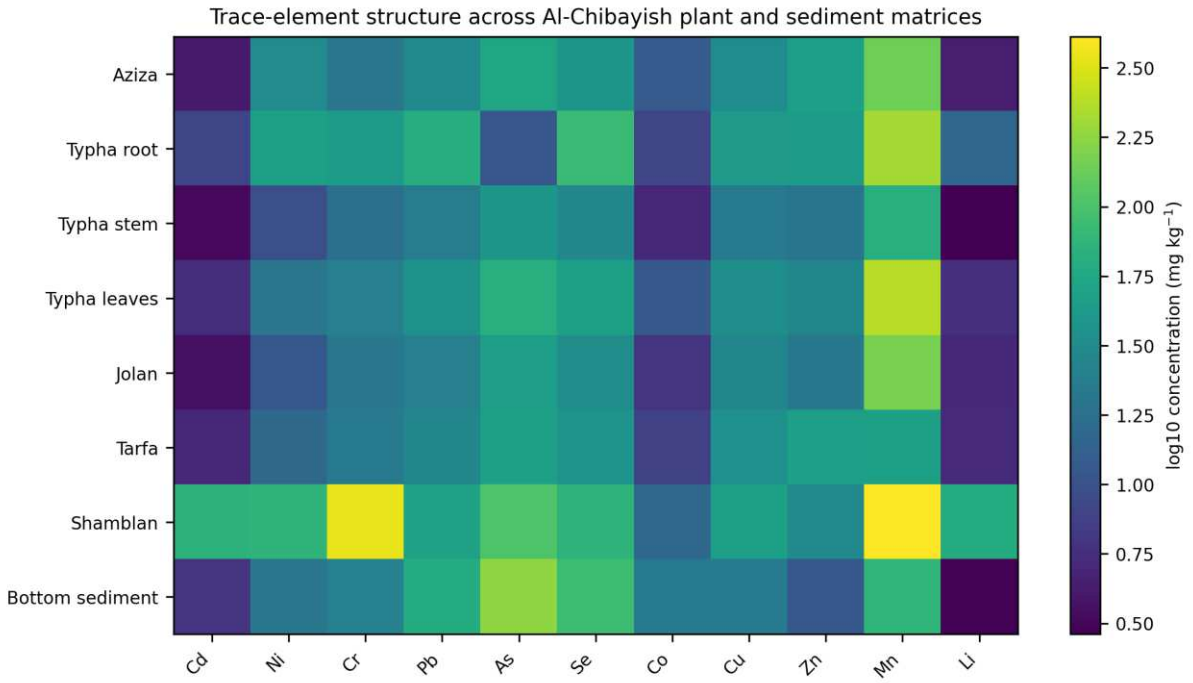


Fig. 1. Log-transformed trace-element structure across the eight Al-Chibayish matrices. The figure is derived only from the supplied elemental dataset.

3.2 Major elements and proximate composition

Major elements and proximate composition separated the mineral-rich bottom sediment from the plant matrices. Bottom sediment had the highest Ca and ash and very low carbohydrate content, whereas Aziza had the highest organic-matter indicator and Tarfa had the highest Na concentration.

Table 3. Major elements (mg kg-1) and proximate composition (% where applicable).

Sample	Ca	Mg	K	Na	P	N %	Protein %	Carbohydrate %	Fiber %	Ash %	Oil %	Moisture %	MO
Aziza	10460	4720	32200	22300	4720	3.82	23.88	41.18	10.15	16.4	0.26	8.13	120.1
Typha root	25080	11550	14200	12100	2680	1.06	6.65	41.8	18.52	28.54	0.19	4.3	28.2
Typha stem	5771	3807	20800	29500	2100	1.4	6.65	41.97	29.62	16.3	0.16	5.3	11.9
Typha leaves	10610	7099	26100	29700	2180	1.22	6.65	30.9	27.36	30.04	0.15	4.9	20.8
Jolan	10840	1764	15100	16300	1780	2.51	15.71	57	9.27	13.08	0.39	4.55	9.8
Tarfa	2341	12310	13400	36000	6450	2.2	6.65	30.9	27.36	30.04	0.15	4.9	14.1
Shamblan	29170	10930	13800	9940	1810	2.05	12.81	5.38	28.2	47.7	0.35	4.56	21.1
Bottom sediment	63350	3285	21500	9420	2090	1.3	8.15	0.98	30.31	55.48	0.28	4.8	22.4

3.3 Matrix-specific maxima

Table 4. Matrix-specific maxima and supplied LSD0.05 thresholds.

Variable	Maximum matrix	Maximum value	LSD0.05
Cd	Shamblan	70.6	0.51
Ni	Shamblan	73.6	23.82
Li	Shamblan	61.8	1.08
Cu	Shamblan	48.1	10.23
Mn	Shamblan	409	34.11
Cr	Shamblan	352	14.06
Fe	Typha root	7780	76.31
Pb	Typha root	63.8	14.55
As	Bottom sediment	179	9.03
Se	Bottom sediment	88.6	17.41
Co	Bottom sediment	21.9	2.08
Ca	Bottom sediment	63350	83.04
Na	Tarfa	36000	64.02
K	Aziza	32200	93.16
P	Tarfa	6450	59.77

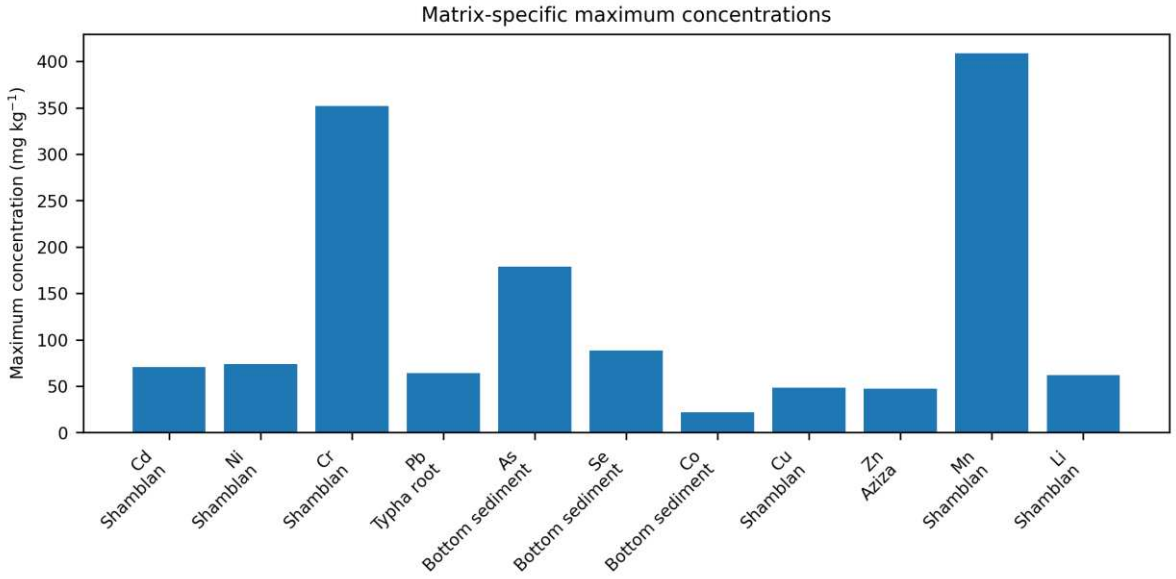


Fig. 2. Matrix-specific maximum concentrations for key trace elements.

3.4 Plant-sediment quotients

Table 5. Highest plant-sediment quotient by element. PSQ = Cplant/Cbottom sediment.

Element	Highest plant matrix	Highest PSQ
Cd	Shamblan	11.55
Ni	Shamblan	3.56
Li	Shamblan	20.81
Cu	Shamblan	2.19
Mn	Shamblan	5.46
Cr	Shamblan	13.59
Fe	Typha root	11.13
Pb	Typha root	1.04
As	Shamblan	0.59
Se	Typha root	0.96
Zn	Aziza	4.15
Co	Shamblan	0.7

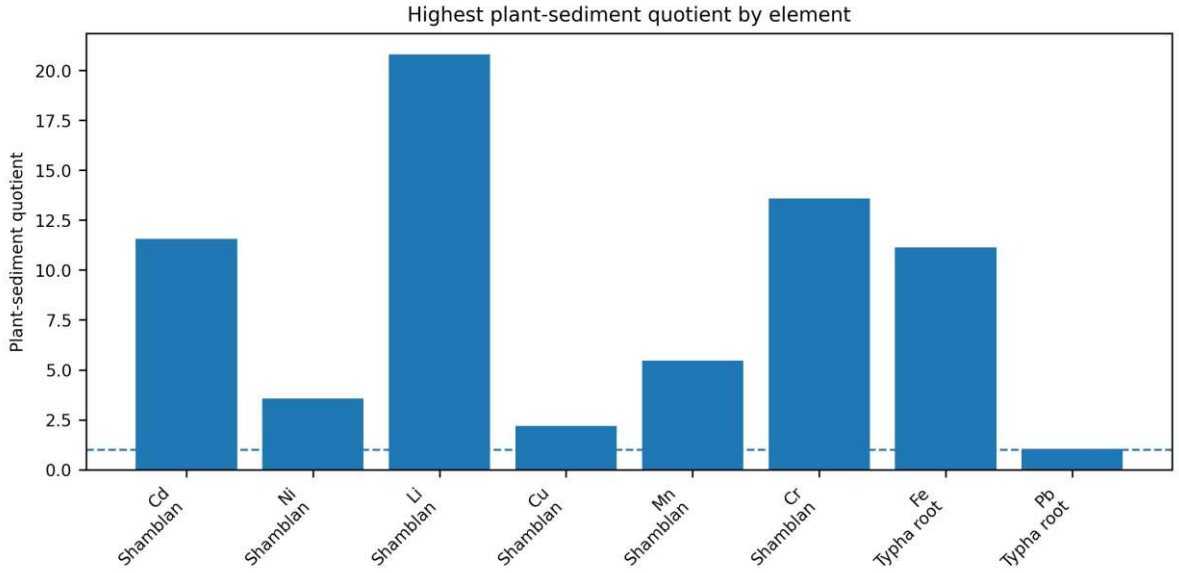


Fig. 3. Highest plant-sediment quotients for selected elements.

3.5 Typha internal partitioning

The Typha root-stem-leaf comparison showed strong root retention for Fe, Cr, Pb, Ni and Ca. Leaves were relatively enriched for Mn and Co compared with roots. This internal partitioning supports separate reporting of roots, stems and leaves rather than combining them as one Typha sample.

Table 6. Internal partitioning among Typha root, stem and leaves.

Element	Root	Stem	Leaves	Stem/root	Leaves/root
Fe	7780	862	2770	0.11	0.36
Cr	43.9	17.9	25.2	0.41	0.57
Pb	63.8	23.3	36.9	0.37	0.58
Cd	8.13	3.28	5.48	0.4	0.67
Ni	48.7	9.6	20.6	0.2	0.42
As	11	39.9	65.5	3.63	5.95
Mn	211	64.1	240	0.3	1.14
Zn	44.6	19.7	27.9	0.44	0.63
Cu	41.7	22.2	33.9	0.53	0.81
Ca	25080	5771	10610	0.23	0.42
Na	12100	29500	29700	2.44	2.45

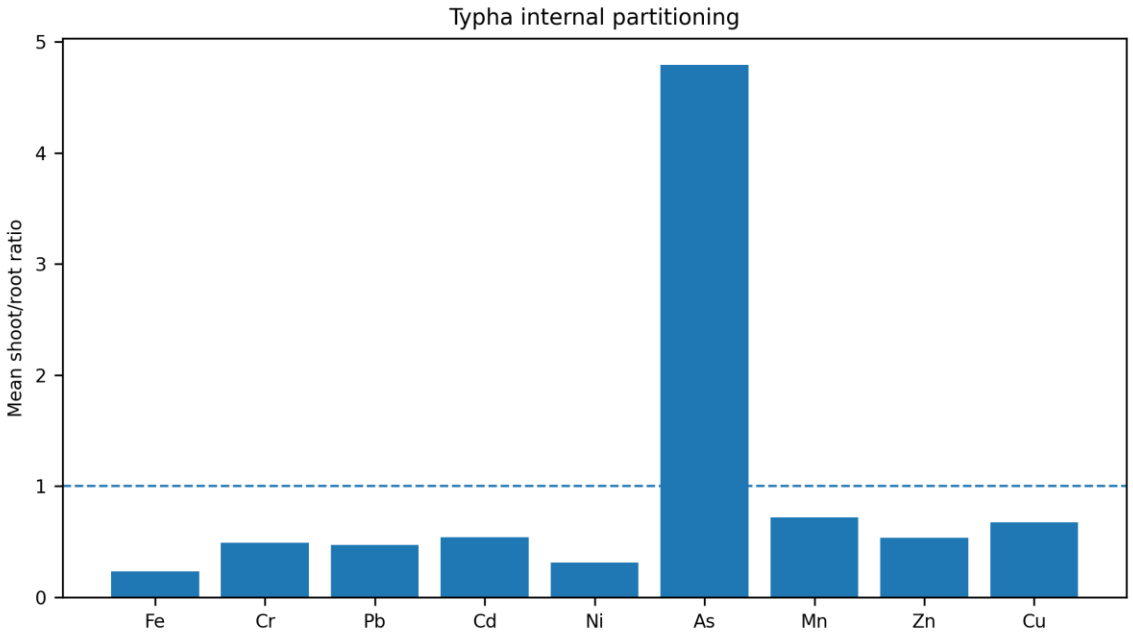


Fig. 4. Mean shoot/root ratios for selected elements in Typha matrices.

3.6 Exploratory multivariate structure

Exploratory PCA separated Shamblan along the trace-element enrichment axis and Bottom sediment along a mineral/metalloid storage axis. Because the sample number is limited, PCA is interpreted as an ordination summary rather than an independent inferential test.

Table 7. Exploratory PCA eigenvalues and component interpretation.

Component	Eigenvalue	Variance %	Cumulative %	Interpretation
PC1	8.11	45.05	45.05	general trace-element enrichment axis
PC2	4.14	23	68.06	carbonate/metalloid/mineral-storage contrast
PC3	2.37	13.17	81.22	nutrient/organic-matter contrast
PC4	1.45	8.08	89.3	minor residual structure
PC5	1.23	6.81	96.11	minor residual structure

Table 8. Exploratory PCA scores for the eight matrices.

Sample	PC1	PC2	PC3
Aziza	-0.85	-0.7	-3.01
Typha root	3	-1.67	0.17
Typha stem	-3.52	0.14	1.18
Typha leaves	-0.09	-0.16	-0.45
Jolan	-1.98	0.67	2.05
Tarfa	-1.96	-2.62	-0.07
Shamblan	5.18	0.04	0.99
Bottom sediment	0.21	4.29	-0.85

Table 9. PCA loadings for elemental variables.

Element	PC1 loading	PC2 loading
Zn	0.2	-0.92

Cu	0.77	-0.6
Ni	0.94	-0.15
Co	0.57	0.55
Fe	0.71	-0.44
Mn	0.78	-0.06
Cr	0.88	-0.03
Ca	0.65	0.7
Mg	0.55	-0.63
K	-0.33	0.29
Na	-0.71	-0.55
Li	0.89	-0.28
Pb	0.8	0.32
Cd	0.89	0
Mo	0.24	-0.09
Se	0.82	0.35
As	0.03	0.69
P	-0.27	-0.6

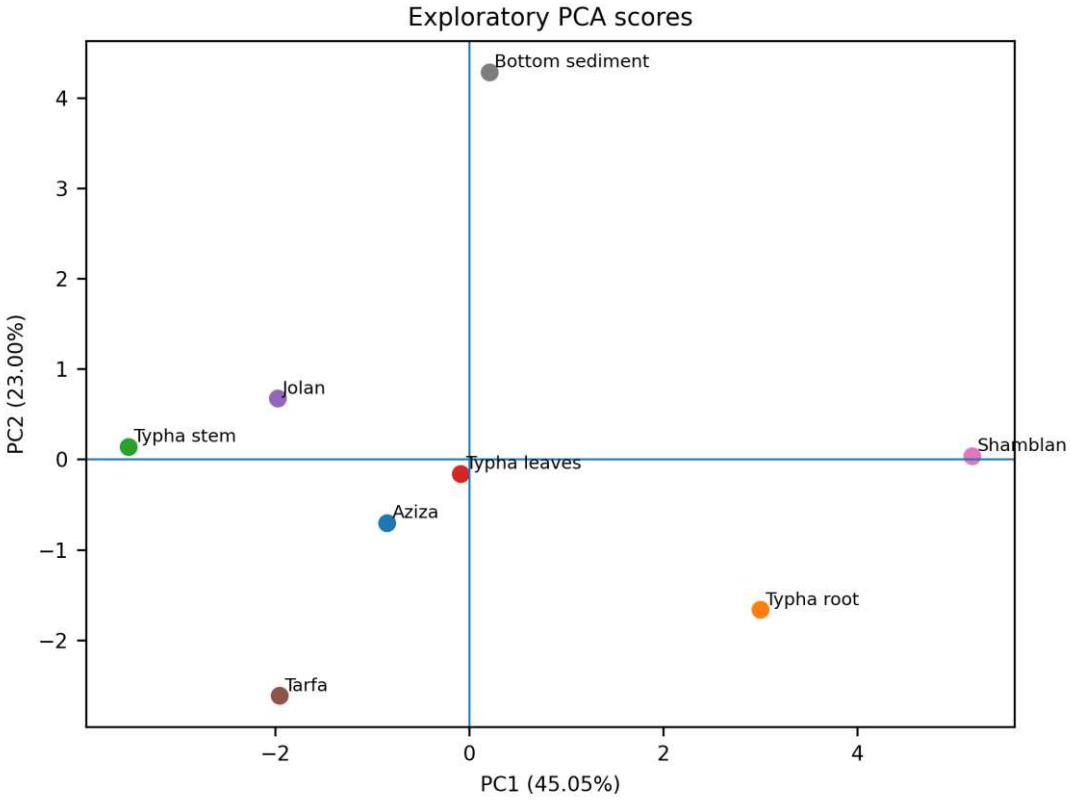


Fig. 5. Exploratory PCA score plot.

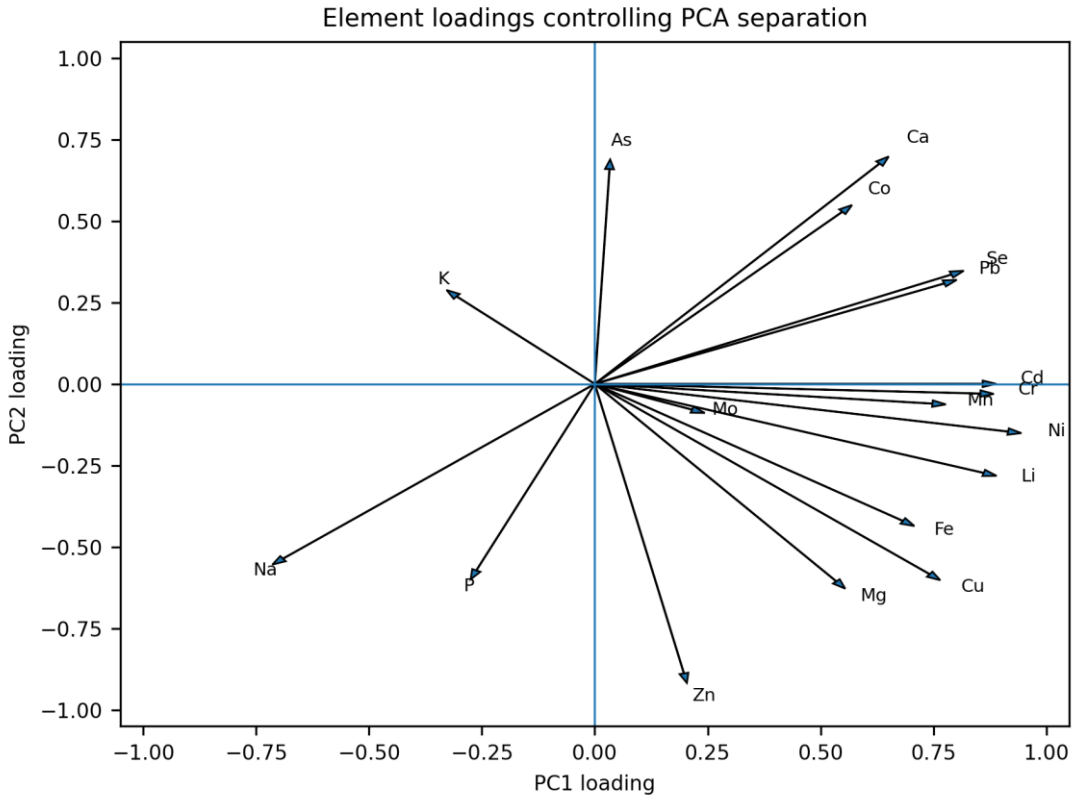


Fig. 6. PCA loading plot for elemental variables.

3.7 Correlation and cross-media models

The correlation matrix showed coherent element associations, including Pb-Se, Cr-Cd, Cr-Li and Li-Cd positive associations, and negative Ca-Na and Na-Se relationships. Cross-media regression models supplied in the workbook were retained as exploratory mathematical summaries, not as spatial prediction models.

Table 10. Strongest positive and negative correlations in the log-transformed plant-sediment matrix.

Element pair	r
Pb-Se	1
Cr-Cd	0.99
Cr-Li	0.95
Li-Cd	0.93
Cu-Li	0.88
Ni-Li	0.83
Ni-Cd	0.81
Ni-Cr	0.8
Ca-Na	-0.92
Na-Se	-0.8
Na-Pb	-0.78
Ca-P	-0.6
Fe-As	-0.59
Ni-Na	-0.59

Table 11. Exploratory cross-media regression models supplied in the statistical workbook.

Model	n	Equation	R2	Adjusted R2	RMSE	LOO RMSE	LOO Q2
All common elements	17	log10(Cplant_mean) = 0.811 + 0.417	0.86	0.84	0.45	0.53	0.8

		log10(Csed) + 0.426 log10(Cwater)					
Trace metals only	12	log10(Cplant_mean) = 1.067 + 0.361 log10(Csed) + 0.088 log10(Cwater)	0.52	0.42	0.4	0.72	-0.55

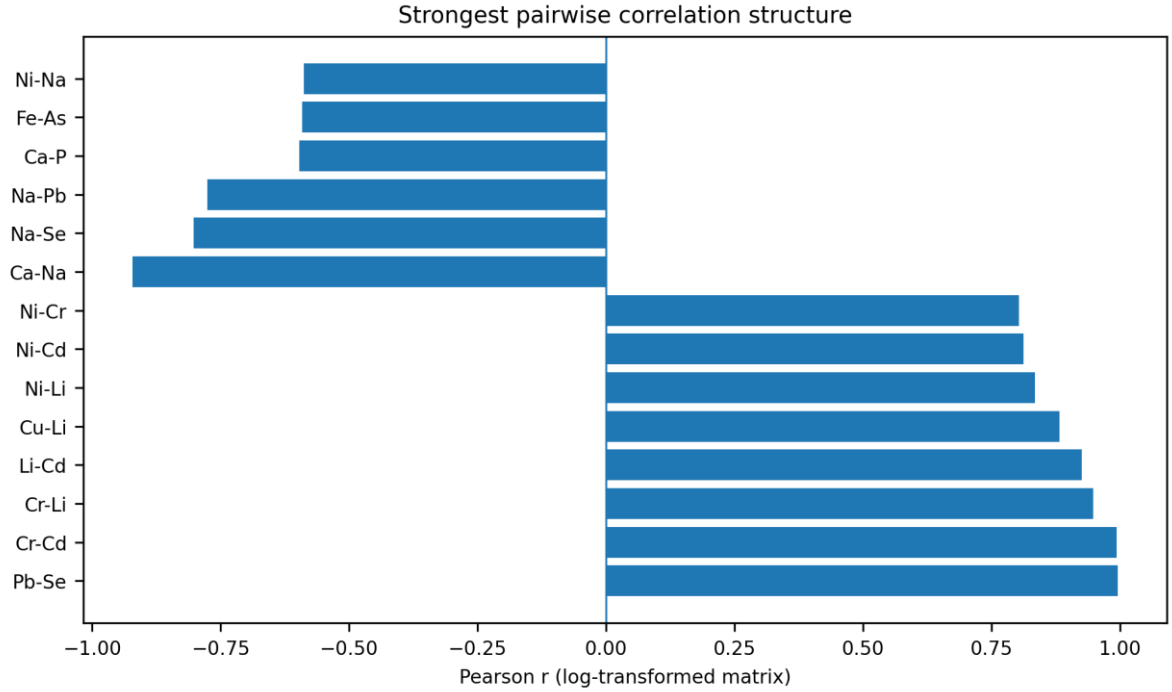


Fig. 7. Strongest pairwise correlation structure.

3.8 FTIR spectral evidence

Original Tensor 27 spectra show repeated bands in regions assigned to hydroxyl, aliphatic, carbonyl/amide, ether/methoxy and fingerprint-region features. Pairwise FTIR comparison figures document differences among Aziza, Typha tissues and other marsh matrices. These features are interpreted as functional-group evidence for organic-matter transformation and contaminant-binding potential.

Table 12. FTIR functional regions used for conservative interpretation.

Region	Functional assignment	Spectral meaning	Geochemical relevance
3600-3200 cm-1	O-H / N-H stretching	hydroxyl-rich biomass, bound water and polar organic groups	metal complexation and hydrogen bonding
2920-2850 cm-1	aliphatic C-H	waxes, lipids and plant polymers	hydrophobic partitioning domain
1740-1600 cm-1	carbonyl, ester, amide	oxidized organic matter and protein-like structures	metal binding and transformation indicator
1540-1500 cm-1	amide/aromatic region	lignocellulosic and protein-related signals	humification screening
1250-1000 cm-1	ether/methoxy/polysaccharide region	plant residue transformation	organic-matter stabilization
900-600 cm-1	fingerprint region	organic-mineral discrimination	mineral-associated matrix evidence

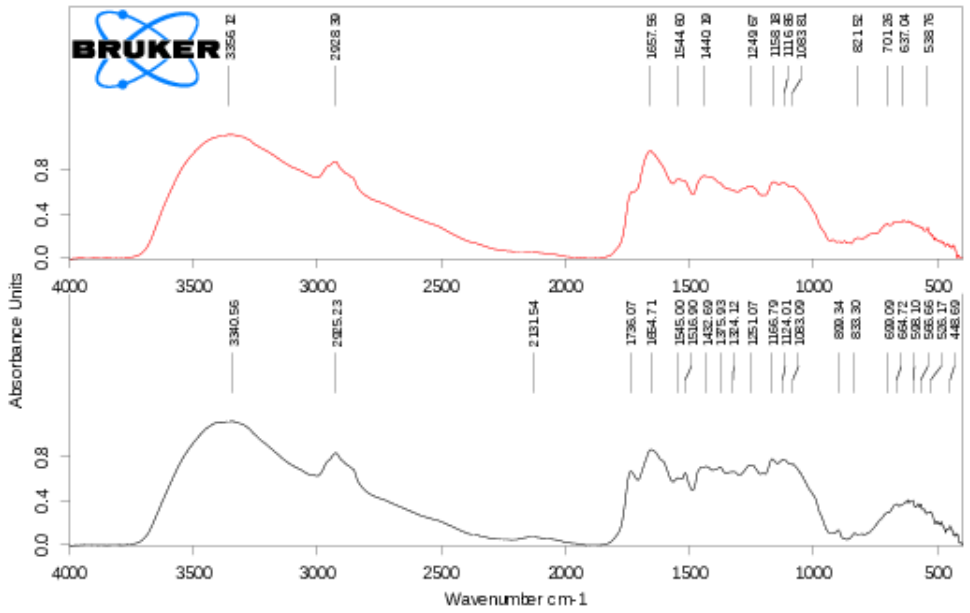


Fig. 8. Original Tensor 27 FTIR comparison between Aziza and Jolan. The figure is retained as an original spectral record and interpreted at functional-group level.

3.9 Remote-sensing and wetting-drying context

Remote-sensing indicators summarized the hydrological setting in which retention and exposure occur. NDVI and NDMI describe vegetation vigor and moisture; NDWI/MNDWI describe surface-water presence; LST and BSI describe thermal and sediment-exposure stress; inundation and exposure frequencies summarize the wetting-drying sequence. These layers support interpretation of environmental conditions but are not used as chemical measurements.

Table 13. Remote-sensing indicators retained as hydrological context.

Indicator	What it represents	Use in this manuscript
NDVI	vegetation density and persistence	organic input and plant-mediated retention
NDWI/MNDWI	surface-water presence	inundation and particle deposition
NDMI	vegetation or sediment moisture	reduced exposure and organic-matter preservation
LST	surface thermal stress	drying intensity and oxidation tendency
BSI	bare/exposed substrate	sediment exposure and possible resuspension
Inundation frequency	recurring water coverage	burial and reducing conditions
Sediment exposure frequency	recurring drying/exposure	drying-rewetting and redistribution risk

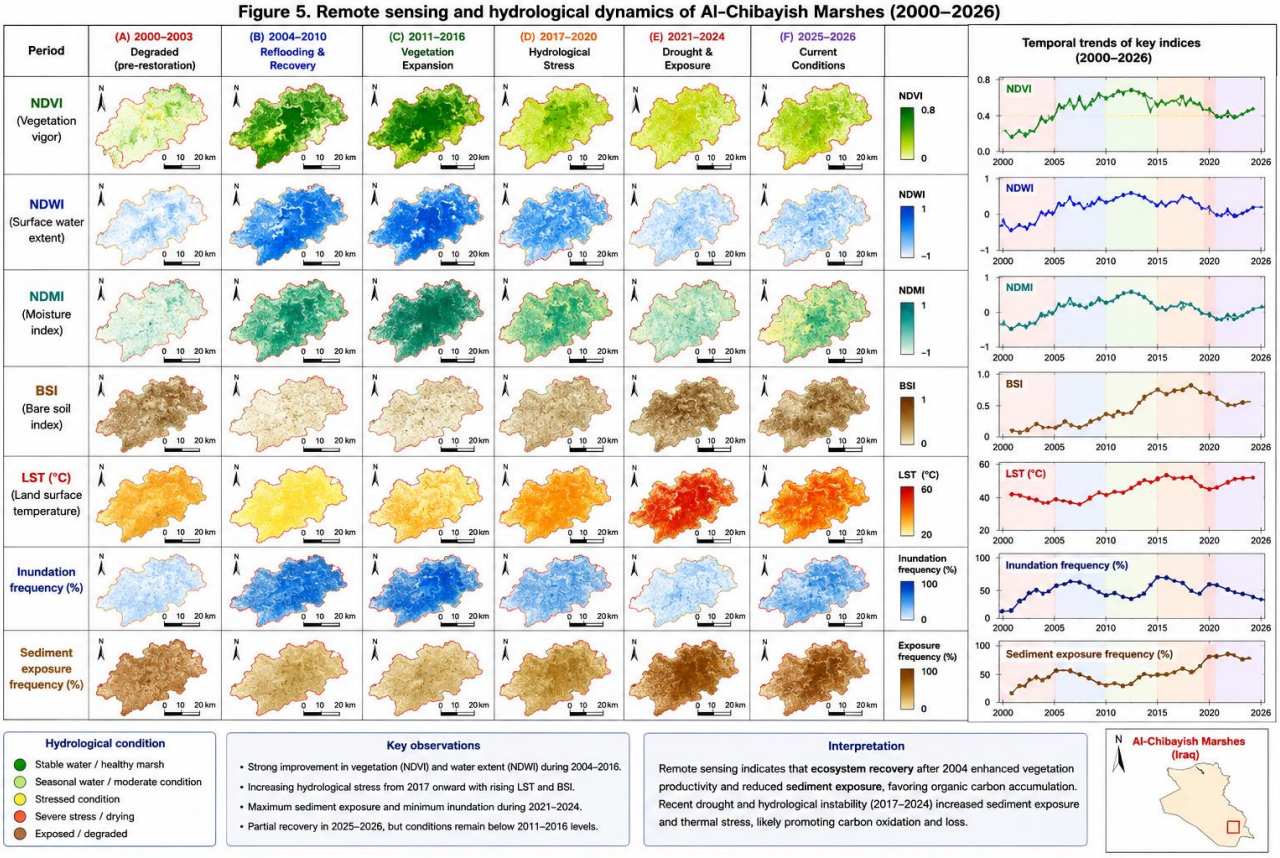


Fig. 9. Original remote-sensing summary of vegetation, water, moisture, thermal stress, bare-soil exposure, inundation and sediment exposure dynamics from the supplied draft. It is used only as environmental context.

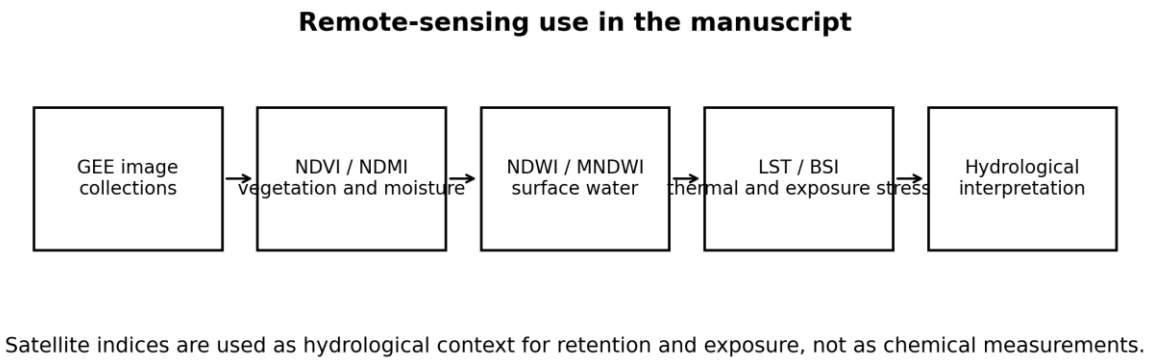


Fig. 10. Restricted role of remote-sensing information in this manuscript.

4. Discussion

The revised results support a restrained interpretation: Al-Chibayish Marshes operate as a plant-sediment retention system in which different matrices concentrate different element groups. Shamblan expresses the strongest submerged-macrophyte signal for Cd, Ni, Li, Cu and Mn; Typha root expresses a rhizosphere interception signal for Fe, Cr and Pb; Bottom sediment expresses mineral-rich storage for As, Se, Co, Ca and ash.

The high Cd and Li quotients in Shamblan are particularly important because they indicate plant-associated enrichment far above the bottom sediment values. This does not by itself separate internal uptake from surface-bound particles. It does, however, identify the submerged macrophyte as a sensitive matrix for monitoring the water-particle-biofilm interface. The elevated Mn is consistent with a redox-sensitive system, since Mn can be mobilized and reprecipitated during changes in oxygen exposure and water level [26-31].

Typha root showed the clearest Fe-Cr-Pb interception signal. Root surfaces in wetland plants commonly form chemically active zones where Fe and Mn phases, organic coatings, biofilms and sediment particles interact. This can concentrate trace elements at the root-sediment boundary and explains why root, stem and leaf matrices should not be pooled. In the current dataset, root enrichment is especially clear for Fe and Cr, whereas Mn and Co show stronger leaf expression.

Bottom sediment differed from plant matrices by its As-Se-Co-Ca-ash signature. This pattern supports a mineral-rich depositional compartment rather than a fresh plant matrix. Ca and ash indicate a strong mineral contribution, whereas As and Se point to metalloid storage under sedimentary control. Such storage can be stable during inundation but may change during exposure, oxidation and salinity concentration [32-36].

FTIR evidence strengthens the interpretation by showing that the matrices contain functional groups capable of sorption and complexation. Hydroxyl, carbonyl/amide and ether/methoxy structures provide polar binding environments, while aliphatic domains and fingerprint-region complexity reflect plant-derived organic matter and organo-mineral transformation. The spectra support a functional model of binding capacity; they do not assign individual organic molecules.

The remote-sensing component is therefore useful only in a specific way. It does not measure contamination. It provides hydrological context for why retention, burial, exposure and redistribution may change through time. Wetting promotes deposition, organic-matter preservation and reducing conditions. Drying exposes sediment, increases thermal stress, concentrates salts and may alter redox-sensitive element behavior. This wetting-drying framing is consistent with the observed need to evaluate plants, roots and sediment as coupled matrices rather than isolated compartments.

5. Conceptual model

The conceptual model links four compartments: water and suspended particles, Shamblan as a submerged biological accumulator, Typha root as a root-zone interception compartment, and Bottom sediment as a mineral-rich sink. Element retention is strongest when inundation maintains contact among suspended particles, biomass and sediment. Redistribution risk increases when sediment exposure and drying-rewetting change the redox and salinity environment.

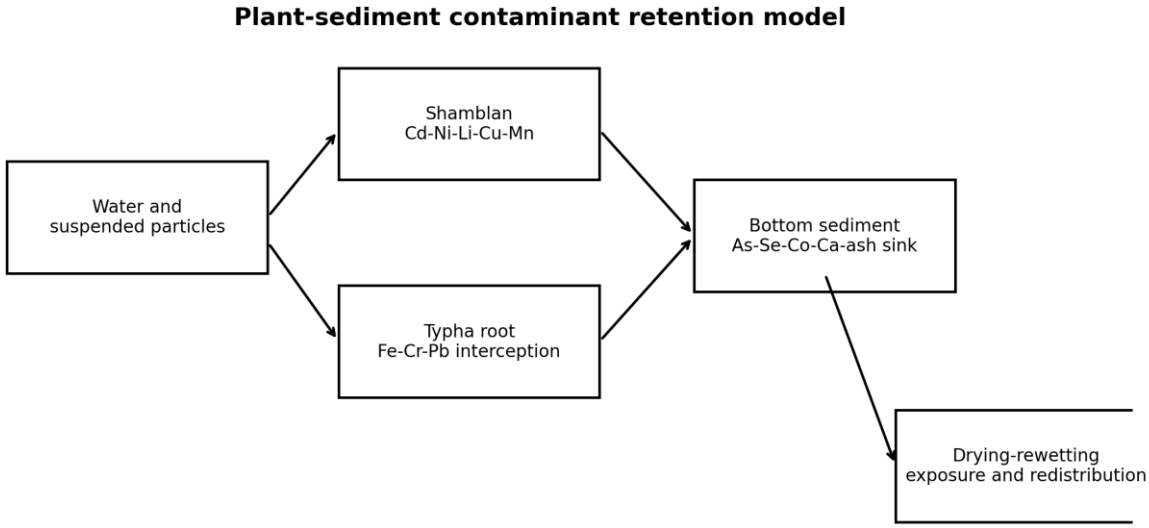


Fig. 11. Conceptual plant-sediment model for trace-element retention and redistribution in Al-Chibayish Marshes.

Table 14. Summary of the proposed plant-sediment retention model.

Model component	Main matrix	Dominant signal	Interpretation
Submerged macrophyte compartment	Shamblan	Cd, Ni, Li, Cu, Mn	plant-associated accumulation
Root interception compartment	Typha root	Fe, Cr, Pb	rhizosphere and root-surface retention
Sediment sink compartment	Bottom sediment	As, Se, Co, Ca, ash	mineral-rich depositional storage
Hydrological control	inundation/exposure sequence	all redox-sensitive pools	retention during wet phases; redistribution during exposure

6. Environmental implications

Table 15. Environmental implications for Al-Chibayish monitoring and interpretation.

Application	Implication
Monitoring design	Report submerged macrophytes, roots and bottom sediment separately.
Sediment assessment	Include metalloid-rich and mineral-rich sediment as a priority matrix.

Plant monitoring	Use Shamblan as a sensitive plant-associated matrix for Cd-Ni-Li-Cu-Mn screening.
Root-zone interpretation	Treat Typha root as a separate Fe-Cr-Pb interception compartment.
Remote-sensing context	Use NDVI, NDWI/MNDWI, NDMI, LST, BSI and exposure frequency to define wetting-drying conditions.
Risk interpretation	Avoid conclusions from water or satellite data alone; use combined plant-sediment evidence.

The practical implication is that the marsh should be monitored as a coupled plant-sediment system. A single matrix cannot describe the system reliably. Submerged plants, roots and bottom sediment provide different but complementary evidence of retention, interception and storage.

7. Limitations

The study is limited by the available analytical package. The elemental table provides final concentrations and LSD thresholds, but the manuscript file does not include raw replicate sheets, digestion records, calibration information, detection limits or certified-reference-material recoveries. FTIR spectra provide functional-group evidence rather than individual molecular assignments. Remote-sensing outputs provide hydrological context and are not used as chemical measurements. These limitations are reflected in the interpretation and prevent overextension beyond the supplied data.

8. Conclusions

- Shamblan (Ceratophyllum sp.) was the strongest plant-associated matrix for Cd, Ni, Li, Cu and Mn.

- Bottom sediment was the dominant matrix for As, Se, Co, Ca and ash, indicating mineral-rich depositional storage.

- Typha root showed a distinct Fe-Cr-Pb interception signal and should be treated separately from Typha stem and leaves.

- FTIR spectra support a functional-group model of organic-matter transformation and contaminant-binding capacity, without assigning individual organic molecules.

- Remote-sensing indicators support the wetting-drying interpretation by documenting vegetation, water, moisture, thermal and exposure conditions.

- The most defensible model is a plant-sediment retention system that can shift under exposure, oxidation and drying-rewetting cycles.

Data availability

The elemental worksheet, FTIR spectral figures and remote-sensing outputs used in this manuscript are available from the corresponding author and can be supplied as supplementary materials. Derived calculations in the manuscript can be reproduced from the tabulated concentrations and the equations stated above.

Declarations

Funding: The author declares that no specific funding was received for this work.

Ethics, Consent to Participate, and Consent to Publish declarations: Not applicable.

Author contribution: R.S.M. designed the study, generated the laboratory dataset, interpreted the results and prepared the manuscript.

References

1. Richardson CJ, Hussain NA. Restoring the Garden of Eden: an ecological assessment of the marshes of Iraq. BioScience. 2006;56:477-489.

2. Partow H. The Mesopotamian Marshlands: Demise of an Ecosystem. UNEP/GRID-Geneva; 2001.

3. Reddy KR, DeLaune RD. Biogeochemistry of Wetlands: Science and Applications. CRC Press; 2008.

4. Mitsch WJ, Gosselink JG. Wetlands. 5th ed. Wiley; 2015.

5. Kadlec RH, Wallace SD. Treatment Wetlands. 2nd ed. CRC Press; 2009.

6. Vymazal J. Constructed wetlands for wastewater treatment: five decades of experience. Environmental Science & Technology. 2011;45:61-69.

7. Bridgham SD, Megonigal JP, Keller JK, Bliss NB, Trettin C. The carbon balance of North American wetlands. Wetlands. 2006;26:889-916.

8. Lehmann J, Kleber M. The contentious nature of soil organic matter. Nature. 2015;528:60-68.

9. Schmidt MWI, Torn MS, Abiven S, Dittmar T, Guggenberger G, Janssens IA, et al. Persistence of soil organic matter as an ecosystem property. Nature. 2011;478:49-56.

10. Kleber M, Sollins P, Sutton R. A conceptual model of organo-mineral interactions in soils. Biogeochemistry. 2007;85:9-24.

11. Lalonde K, Mucci A, Ouellet A, Gelinas Y. Preservation of organic matter in sediments promoted by iron. Nature. 2012;483:198-200.

12. Kogel-Knabner I. The macromolecular organic composition of plant and microbial residues as inputs to soil organic matter. Soil Biology and Biochemistry. 2002;34:139-162.

13. Cotrufo MF, Wallenstein MD, Boot CM, Denef K, Paul E. The microbial efficiency-matrix stabilization framework integrates plant litter decomposition with soil organic matter stabilization. Global Change Biology. 2013;19:988-995.

14. Parikh SJ, Goyne KW, Margenot AJ, Mukome FND, Calderon FJ. Soil chemical insights provided through vibrational spectroscopy. Advances in Agronomy. 2014;126:1-148.

15. Madejova J. FTIR techniques in clay mineral studies. Vibrational Spectroscopy. 2003;31:1-10.

16. Socrates G. Infrared and Raman Characteristic Group Frequencies. 3rd ed. Wiley; 2001.

17. Tessier A, Campbell PGC, Bisson M. Sequential extraction procedure for the speciation of particulate trace metals. Analytical Chemistry. 1979;51:844-851.

18. Rauret G, Lopez-Sanchez JF, Sahuquillo A, Rubio R, Davidson C, Ure A, Quevauviller P. Improvement of the BCR three step sequential extraction procedure prior to certification of new sediment and soil reference materials. Journal of Environmental Monitoring. 1999;1:57-61.

19. Hakanson L. An ecological risk index for aquatic pollution control: a sedimentological approach. Water Research. 1980;14:975-1001.

20. Muller G. Index of geoaccumulation in sediments of the Rhine River. Geojournal. 1969;2:108-118.

21. Tomlinson DL, Wilson JG, Harris CR, Jeffrey DW. Problems in the assessment of heavy-metal levels in estuaries and the formation of a pollution index. Helgolander Meeresuntersuchungen. 1980;33:566-575.

22. Long ER, MacDonald DD, Smith SL, Calder FD. Incidence of adverse biological effects within ranges of chemical concentrations in marine and estuarine sediments. Environmental Management. 1995;19:81-97.

23. MacDonald DD, Ingersoll CG, Berger TA. Development and evaluation of consensus-based sediment quality guidelines for freshwater ecosystems. Archives of Environmental Contamination and Toxicology. 2000;39:20-31.

24. Canadian Council of Ministers of the Environment. Canadian sediment quality guidelines for the protection of aquatic life: summary tables. CCME; 2001.

25. Alloway BJ. Heavy Metals in Soils: Trace Metals and Metalloids in Soils and their Bioavailability. Springer; 2013.

26. Kabata-Pendias A. Trace Elements in Soils and Plants. 4th ed. CRC Press; 2011.

27. Du Laing G, Rinklebe J, Vandecasteele B, Meers E, Tack FMG. Trace metal behaviour in estuarine and riverine floodplain soils and sediments: a review. Science of the Total Environment. 2009;407:3972-3985.

28. Rinklebe J, Shaheen SM. Redox chemistry of nickel in soils and sediments: a review. Chemosphere. 2017;179:265-278.

29. Smedley PL, Kinniburgh DG. A review of the source, behaviour and distribution of arsenic in natural waters. Applied Geochemistry. 2002;17:517-568.

30. Masscheleyn PH, Delaune RD, Patrick WH. Effect of redox potential and pH on arsenic speciation and solubility in a contaminated soil. Environmental Science & Technology. 1991;25:1414-1419.

31. Uddin MK. A review on the adsorption of heavy metals by clay minerals, with special focus on the past decade. Chemical Engineering Journal. 2017;308:438-462.

32. Bolan N, Kunhikrishnan A, Thangarajan R, Kumpiene J, Park J, Makino T, et al. Remediation of heavy metal(loid)s contaminated soils: to mobilize or to immobilize? Journal of Hazardous Materials. 2014;266:141-166.

33. Ali H, Khan E, Sajad MA. Phytoremediation of heavy metals: concepts and applications. Chemosphere. 2013;91:869-881.

34. Salt DE, Smith RD, Raskin I. Phytoremediation. Annual Review of Plant Physiology and Plant Molecular Biology. 1998;49:643-668.

35. Weis JS, Weis P. Metal uptake, transport and release by wetland plants: implications for phytoremediation and restoration. Environment International. 2004;30:685-700.

36. Bonanno G, Vymazal J, Cirelli GL. Translocation, accumulation and bioindication of trace elements in wetland plants. Science of the Total Environment. 2018;631-632:252-261.

37. Marchand L, Mench M, Jacob DL, Otte ML. Metal and metalloid removal in constructed wetlands, with emphasis on the importance of plants and standardized measurements. Environmental Pollution. 2010;158:3447-3461.

38. Stottmeister U, Wiessner A, Kuschk P, Kappelmeyer U, Kastner M, Bederski O, et al. Effects of plants and microorganisms in constructed wetlands for wastewater treatment. Biotechnology Advances. 2003;22:93-117.

39. Tucker CJ. Red and photographic infrared linear combinations for monitoring vegetation. Remote Sensing of Environment. 1979;8:127-150.

40. McFeeters SK. The use of the Normalized Difference Water Index in the delineation of open water features. International Journal of Remote Sensing. 1996;17:1425-1432.

41. Gao B. NDWI: a normalized difference water index for remote sensing of vegetation liquid water from space. Remote Sensing of Environment. 1996;58:257-266.

42. Xu H. Modification of normalized difference water index to enhance open water features in remotely sensed imagery. International Journal of Remote Sensing. 2006;27:3025-3033.

43. Pettorelli N, Vik JO, Mysterud A, Gaillard JM, Tucker CJ, Stenseth NC. Using the satellite-derived NDVI to assess ecological responses to environmental change. Trends in Ecology & Evolution. 2005;20:503-510.

44. Gorelick N, Hancher M, Dixon M, Ilyushchenko S, Thau D, Moore R. Google Earth Engine: planetary-scale geospatial analysis for everyone. Remote Sensing of Environment. 2017;202:18-27.

45. Huete AR. A soil-adjusted vegetation index. Remote Sensing of Environment. 1988;25:295-309.

46. Avdan U, Jovanovska G. Algorithm for automated mapping of land surface temperature using Landsat 8 satellite data. Journal of Sensors. 2016;2016:1480307.

47. Zha Y, Gao J, Ni S. Use of normalized difference built-up index in automatically mapping urban areas from TM imagery. International Journal of Remote Sensing. 2003;24:583-594.

48. Amani M, Mahdavi S, Afshar M, Brisco B, Huang W, Mirzadeh SMJ, et al. Canadian wetland inventory using Google Earth Engine. Remote Sensing. 2019;11:842.

Supplementary Files

This is a list of supplementary files associated with this preprint. Click to download.

- Supplementarymaterial.doc